Analysis of current-voltage characteristics of Fe/MgO/GaAs junctions using self-consistent field modeling

Y. J. Park,[1,2,*] M. C. Hickey,[1,†] M. J. Van Veenhuizen,[1] J. Chang,[1,2] D. Heiman,[3] and J. S. Moodera[1]
[1]*Francis Bitter Magnet Laboratory, Massachusetts Institute of Technology, 150 Albany Street, Cambridge, Massachusetts 02139, USA*
[2]*Center for Spintronics Research, Korea Institute of Science and Technology, Seoul, Korea*
[3]*Department of Physics, Northeastern University, Boston, Massachusetts 02115, USA*
(Received 14 April 2009; revised manuscript received 28 September 2009; published 14 December 2009)

Current-voltage data in metal-insulator-semiconductor devices are usually interpreted by a model of the tunneling current or the Schottky thermionic emission current. In these models, the barrier through which the electrical current flows is normally assumed to be rectangular or at best trapezoidal. For metal-insulator-metal junctions, this is a reasonable assumption. However, when one electrode is a doped semiconductor, the parameters of the current-voltage models require a self-consistent field description and the bias-dependent band bending within the semiconductor must be taken into account. These bias-dependent energy-band profiles are modeled with a Schrödinger-Poisson solver and incorporated into the fitting procedure for the current-voltage data. We find that the ratio of the Schottky thermionic emission to the tunneling current, as well as the tunnel barrier heights can be determined using this approach. With this approach, one can quantitatively distinguish between tunneling and thermionic transport regimes and this is particularly applicable to the interpretation of spin-transport experiments in metal-insulator-semiconductor devices.

DOI: 10.1103/PhysRevB.80.245315 PACS number(s): 73.40.−c, 73.30.+y, 73.20.At

I. INTRODUCTION

Metal-insulator-semiconductor (MIS) junctions are ubiquitous devices which underpin much of the functionality of technology which is based on electronic charge. Likewise, they are expected to play a key role in spintronics, wherein the MgO tunnel barrier is an optimal candidate for memory and switching devices.[1–3] In order to inject and detect spin-polarized carriers efficiently in semiconductors, a tunnel barrier is required to avoid the conductivity mismatch and enables the efficient functionality of a spin transistor.[4,5] Evaluating the barrier profile through which electrons flow from metals into semiconductors is of paramount importance in order to quantitatively assess the current-voltage characteristics of these heretostructures. The GaAs/MgO/Fe structure has been considered as a promising candidate for the spin-injection/detection structures with efficient exploitation of spin filtering.[6] In addition to this, the MgO crystal structure is well lattice matched to GaAs, which allows coherent tunneling. The main advantage of the MgO/Fe structure is that it can be prepared epitaxially and forms a basic building block for the magnetic tunnel junction structure of Fe(Co)/MgO/(Co)Fe, yielding giant tunneling magnetoresistance.[7,8] The MgO barriers selectivity of totally symmetric spin up Δ_1 Bloch states in the Fe (Refs. 9 and 10) is the physical basis for coherent-spin tunneling. There has been much theoretical work done on spin-polarization reversal due to surface-state resonance in Fe/GaAs (001) heterostructures[11,12] as well as spin extraction.[13]

Efficient spin filtering has been observed in GaAs/MgO/Fe structures, predominantly in the moderate forward bias region.[6,14,15] The study of current-voltage (*I-V*) characteristics of this type of structure is important for understanding the bias-dependent spin-filtering phenomena. Analysis of MIS structures has been previously made on the basis of the tunneling theory by Card *et al.*[16] That model, however, is not satisfactory for understanding the *I-V* characteristics of present GaAs/MgO/Fe structures. Additional considerations of minority carrier behavior[17] and interface trap dynamics[18] have been reported, but a full understanding of the bias-dependent transport properties of MIS junctions is lacking. A full interpretation of current-voltage data with respect to thermionic and tunneling transport as complimentary mechanisms will improve our understanding of spin-filtering phenomena in these systems.

In this work, we focus on charge transport alone and we report on the analysis of *I-V* characteristics in GaAs/MgO/Fe structures incorporating the use of a self-consistent field (SCF) description of the electric field and charge carrier densities. In order to properly quantify the band bending and its effect on *I-V* characteristics as a function of applied external bias, a more complete picture of the energy states, wave functions and electric fields is needed. For this, we apply the following modeling techniques to analyze the $I(V)$ data: (1) a self-consistent Schrödinger-Poisson band profile solver and (2) parameterization of the Schottky/tunnel barrier model including the calculated dependence of the barrier profiles on applied bias.

II. EXPERIMENT

The (100) GaAs/MgO/Fe structures whose *I-V* characteristics were measured were grown in a UHV chamber by e-beam deposition. The n^+ GaAs(100) was doped with a concentration of 2×10^{18} cm^{-3} and was cleaned in a ultrasonic bath with isopropyl-alcohol and acetone for 3 min each, followed by the removal of native oxide with diluted HCl (1:10 HCl: deionized water) solution for 1 min. The etched substrate was put in the load lock chamber and prebaked at 300 °C and then positioned in the main growth chamber for the deposition of 2.75–3.8 nm MgO/7 nm Fe structure. The base pressure of the UHV chamber was 2×10^{-10} Torr. The

deposition rate of MgO and Fe was 0.1 and 0.2 Å s^{-1} (on GaAs) at room temperature, respectively. Post-annealing at 250 °C for 10 min was performed after the growth. This is a critically important step toward actualizing a smooth interface between the MgO and the crystalline substrate[8] and the annealing temperature is limited to 250 °C in order to limit the interdiffusion of oxygen atoms into the *n*-GaAs.[19] Finally, the 4-nm-thick Au was deposited as a capping layer. The front side indium contacts and the back side ohmic contact (AuGe alloy annealed at 400 °C) were simultaneously connected to a current source and a voltmeter, respectively. It is important for the interface between the MgO and the Fe electrode to have a smooth morphology for the fabrication of spin-injection/detection device applications. In order to get a smooth morphology, a post-annealing process is required. In particular, the generation of pinholes is detrimental to the thin tunnel barrier MIS structure which can sometimes arise due to poor surface coverage of the thin MgO layer on GaAs. From the atomic force microscopy measurements on the surface morphology of the MgO thin tunnel barrier (typically 2–4 nm) as grown on the GaAs substrate, the root-mean square (rms) of surface roughness was found to be approximately 0.25 nm after the thermal annealing. Without the annealing process, the rms of roughness was measured to be as large as 1 nm. For a high-quality MgO thin film, appropriate growth conditions (low deposition rate, post-annealing process, substrate temperature) are crucial.

III. MODELING AND ANALYSIS OF THE *I-V* CHARACTERISTICS

The *I-V* characteristics are analyzed with a model which uses a SCF Schrödinger-Poisson band-profile solver to obtain the bias-dependent tunnel barrier height [TBH(V)], the Schottky barrier height [SBH(V)], the potential drop across the tunnel barrier, and the surface-potential band bending of the semiconductor V_{bb}. These parameters are subsequently modified by the fitting procedures using the Schottky/tunnel barrier model constructed in this study. First, the energy-band bending can be calculated. The most commonly used model for fitting current-voltage [$I(V)$] data for tunneling currents in tunneling heterostructures is the Simmons model. This model is based on the Wentzel-Kramers-Brillouin approximation and the current in this model has the following dependence on applied voltage bias,[20,21]

$$J_T = \frac{qI_0^{\mathrm{TB}}}{4\pi^2\beta^2\hbar d^2}\left[(q\tilde{\phi} - q\tilde{V}/2)\exp\left(-2d\sqrt{\frac{2m_e}{\hbar^2}}\sqrt{q\tilde{\phi} - q\tilde{V}/2}\right)\right.$$
$$\left. - (q\tilde{\phi} + q\tilde{V}/2)\exp\left(-2d\sqrt{\frac{2m_e}{\hbar^2}}\sqrt{q\tilde{\phi} + q\tilde{V}/2}\right)\right]. \quad (1)$$

In the above equation, $\tilde{\phi} = \phi(V) - \phi_0$, which accounts for both an offset in the barrier height (ϕ_0, defined with respect to the Fermi level in the metal) and the voltage dependence of the barrier height. $\tilde{V} = V - V_s$, d is the thickness of the tunnel barrier and β is the inverse of the Boltzmann temperature, while V and V_s are the voltage and electrochemical shift across the barrier, respectively. I_0^{TB}, q, and m_e are the prefactor to estimate the $J_{\mathrm{SB}}/J_{\mathrm{TB}}$ ratio, electronic charge and mass, respectively. This equation necessitates a knowledge of the barrier height ϕ which in general is a functional of the applied bias $\phi([V])$, and gives the deviation from the zero-bias barrier height (averaged over the barrier thickness). This must be accounted for self-consistently because a finite electron density of states arises in the *n*-doped semiconductor and so this affects the space charge electrostatic potential. For the self-consistent energy-band profile analysis, the parameters used in this study are listed in Table I.

TABLE I. Parameter values used in calculation for the MgO/GaAs heterostructure. E_g is the semiconductor gap, m_{eff} is the effective mass, ϵ_r is the relative dielectric permittivity, and T is the Boltzmann temperature.

Material	E_g (eV)	m_{eff}/m_0	m_{eff}^{hh}/m_0	ϵ_r (F m^{-1})	T (K)
GaAs	1.42	0.067	0.51	13.1	300
MgO	7.8[b]	0.35	0.33[c]	7[a]	300

[a]Typical value obtained from capacitance-voltage measurements.
[b]Reference 22.
[c]Reference 23.

The counterpart to this model is the thermionic Schottky current equation which is most commonly written as[24]

$$J_{\mathrm{SB}} = J_0^{\mathrm{SB}}\exp\left(\frac{qV_s}{nk_BT}\right)\left[1 - \exp\left(\frac{-qV_s}{k_BT}\right)\right],$$

where

$$J_0^{\mathrm{SB}} = I_0^{\mathrm{SB}}A^{**}T^2\exp\left(-\frac{q\phi_{\mathrm{SB}}}{k_BT}\right). \quad (2)$$

A^{**} is the Richardson constant, n is the ideality factor, I_0^{SB} is the prefactor to estimate the $J_{\mathrm{SB}}/J_{\mathrm{TB}}$ ratio, which is the ratio of the Schottky current to the tunneling current. The Schottky barrier height Φ_{SB} is given by the following equation

$$\phi_{\mathrm{SB}} = \phi_{\mathrm{SB}}^0 - \gamma_t(V_m - V_s) + \gamma_s V_s, \quad (3)$$

which gives the Schottky barrier height offset which depends on the equilibrium Schottky height (ϕ_{SB}^0) applied voltage (V_m) to the metal contact and also the degree of electrochemical potential drop (V_s) across the Schottky barrier. The systems equilibrium is defined by the condition of zero bias (V_s=0) These three terms in the definition for ϕ_{SB} represent the equilibrium barrier height, the capacitive band bending in the metal/semiconductor interface, and the band banding due to the electrochemical potential drop when the junction is under small forward bias (the case where current is allowed to flow in the semiconductor). The schematic in Fig. 1 shows how these parameters are defined. The constants γ_s and γ_t contain the capacitances per unit area of the barrier junction and are defined as follows:[25]

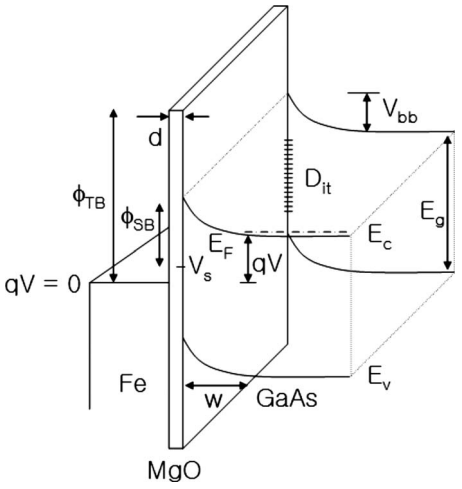

FIG. 1. Schematic energy-band diagram of the metal/insulator/semiconductor junction showing the tunnel/Schottky configuration.

$$\gamma_t = \frac{\tilde{C}_t}{\tilde{C}_t + \tilde{C}_s + q^2 D_{it}}, \quad \gamma_s = \frac{\tilde{C}_s}{\tilde{C}_t + \tilde{C}_s + q^2 D_{it}},$$

where $\tilde{C}_t(\tilde{C}_s)$ are the capacitances per unit area of the tunneling (Schottky) barrier and D_{it} is the surface density of states given in units of J^{-1} m^{-2}.

In order to properly quantify the band bending and dependence of the barrier characteristics as a function of applied external bias, we need to model the metal/insulator/semiconductor system. In order to achieve this, we parameterize the Schottky/tunnel barrier model with the calculated dependencies of the barrier profiles on applied bias from the SCF calculation to achieve accurate fitting of the $I(V)$ data.

The first solver, which in this case is that developed by Tan *et al.*,[26] is used to calculate the wave function of bound electronic states in the quantum well, electron, and hole densities and the band energy of the conduction and valence states in the system. We are interested in the values of these coefficients for the bound electronic states in the quantum well, and so a full description of the quantum-well wave function and the electric field in the vicinity of the well are required. The SCF solver finds the solution of the Poisson equation in order to establish the electrostatic potential and the equilibrium electron space charge density in the device. The electrostatic potential $V(z)$ is initially taken to be given by the pseudopotential band offsets of the materials in the heterostructure and this is plugged into the Schrödinger equation from which the energy eigenvalues and corresponding eigenstates of the bound electrons are calculated

$$-\nabla \cdot \left[\frac{1}{m^*(z)\pi^2}\nabla\Psi\right] - \frac{qV(z)}{E_1}\Psi - \frac{\lambda_E}{E_1}\Psi = 0, \tag{4}$$

where $E_1(=\frac{\hbar^2}{2m_0a^2})$ is a constant related to the first energy eigenvalue in an infinite quantum well, m^* is the effective mass, λ_E is an energy eigenvalue, and z is the coordinate along the growth axis. From the electron wave function calculated above, we can now calculate the total electron density for an electron ensemble with chemical potential μ and at Boltzmann temperature T;

$$n(z) = 2\sum_{j0,m0}\int_{E_{\mathbf{k}}}^{\infty}\frac{d\mathbf{k}}{2\pi}|\Psi_{j0,m0,\mathbf{k}}(z)|^2 f_{FD}(E_{jm\mathbf{k}} - \mu)g(E_{\mathbf{k}}), \tag{5}$$

and the calculated electron number density $n(z)$ is plugged into the Poisson equation, as follows:

$$-\nabla \cdot [\epsilon_r(z) \cdot \nabla V(z)] = \frac{q}{\epsilon_0}[n_D(z) - n(z,V)]. \tag{6}$$

The new self-consistent electrostatic potential arising from the Poisson equation is allowed to converge over successive iterations until the electrostatic potential and electron density is unchanged to within the desired error. A sample of the calculation of the SCF band diagram is shown in Fig. 2 with the numerically defined $I(V)$ model band parameters.

To describe the model at the heart of the fitting process, the equivalent resistive circuit model is constructed. Figure 3 shows the equivalent circuits for the tunnel/Schottky barrier model and its relevant transport band diagram. Fitting parameters can be obtained through the matching process with calculated energy-band profiles on applied bias for the experimental data. In the forward bias region, depending on the effective tunnel barrier height, the current path is composed of three: (1) thermionic emission over or through the effective tunnel barrier, (2) direct tunneling through the MgO tunnel barrier and Schottky barrier, and (3) interface states tunneling as shown in Figs. 3(a) and 3(b). In our simple model, the total current is comprised of a combination of processes (1)–(3), depending on the relative magnitude of the current in each path. The J_{SB} component is comprised of current density in the transport path (2) as well as the path (1) and J_{TB} relates to the transport path (2) and (3). Thus, it is unrealistic that quantitative determination of J_{TB} and J_{SB} is possible through the fitting process. Instead, the ratios of J_{SB}/J_{TB} are obtained to distinguish between the bias-dependent transport process by setting the total current J_T [paths (1), (2), and (3)] $=J_{SB}$ [carried by path (1) and, in part, path (2)] $+J_{TB}$ [carried by path (3) and, in part (2)], resulting from parallel transport. When considering the interface state dynamics,[18] the interface state tunneling varies with the tunneling time constant associated with the thickness and the tunnel barrier height, which depend on the bias. It is unrealistic to quantify them all and this is beyond the scope of this study. However, it is obvious that the interface state tunneling is suppressed in the absence of interface states, whose density is given by D_{it}.

The strength of the SCF approach to the fitting of I-V characteristics of these Fe/MgO/n-GaAs junctions is that it quantitatively accounts for the modulation of the barrier profile and the modification of the bands in order to accurately fit the I-V data. The augmentation afforded by the SCF method gives rise to a functional voltage dependence of $\phi([V])$, $\phi_{SB}([V])$, $V_s([V])$, and $V_{bb}([V])$. In order to demonstrate the advantage of our SCF $I(V)$ model over a rigid band Simmons/Schottky circuit model, we show model fits for both cases in Fig. 4. The comparison shows an improvement

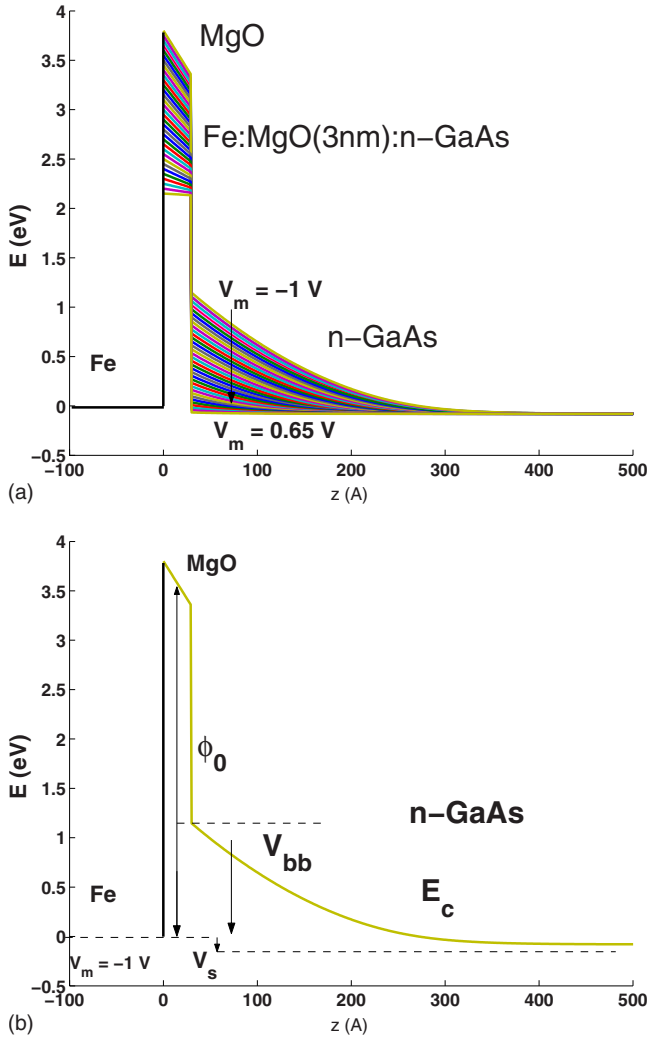

FIG. 2. (Color online) (a) Plot of the conduction-band diagram for the Fe:MgO:*n*-GaAs heterostructure calculated using the self-consistent Schrödinger-Poisson solver code developed by Tan *et al.* (Ref. 26). The bias-voltage scale runs from V_m=−1 to V_m=0.65. From these bands, the functional dependence of ϕ, ϕ_{SB}, $V_s(V)$ on applied bias (V) are calculated. (b) The definition of the self-consistent parameters which parameterize the fit.

in fit convergence by one order of magnitude. Using the present self-consistent model, the data can be fitted by manipulating the calculated parameters for each sample. Particularly, the V_{bb} obtained first from the self-consistent method has been modified through the subsequent fitting process to the experimental data as shown in Fig. 5(a). The resultant fitting curves are plotted together with data in Fig. 5(b). It should be noted here that we adopted a piecewise fit method (i.e., fitting within a specific bias region) to understand which transport process dominates in the given bias region. Moreover, the method can provide a more accurate fit profile compared to a fit over the entire bias range. As shown in Fig. 5(c), the fit appears to converge with the data on a linear scale but shows a massive deviation in the logarithm scale with a whole fit method. It is also interesting to note here that the 3.8-nm-thick MgO sample shows somewhat different *I-V* characteristics compared to the 3.0-nm-thick

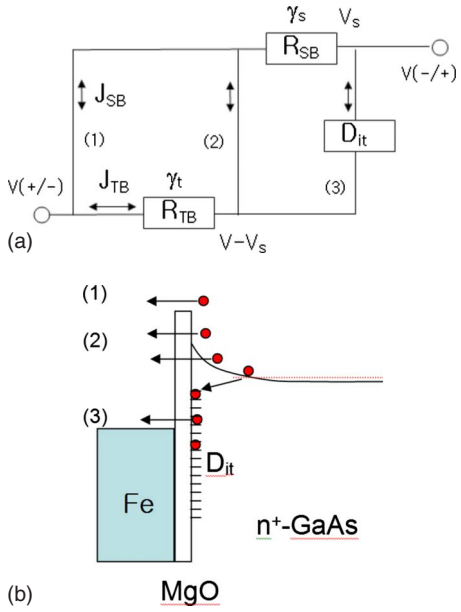

FIG. 3. (Color online) (a) Equivalent circuit of GaAs/MgO/Fe structure on the basis of the self-consistent resistive model. R_{TB}, R_{SB}, and D_{it} correspond to the tunnel barrier resistance, Schottky barrier resistance, and the density of states, respectively. V_s and γ_t are defined in the text. (b) Its relevant transport band diagram in the forward bias region.

MgO sample as shown in Fig. 5(d) indicating a very slowly increasing current with voltage in the low forward bias region. This kind of *I-V* characteristic curve can hardly be fitted using a conventional whole fit method. However, using the present piecewise method, it can be fitted nicely with the data as shown in Fig. 5(d). Thus we propose the piecewise fit method for the fitting of *I-V* curves from which we can quantitatively obtain several physical parameters.

Through the fitting process, the SBH, TBH, the prefactors of I_0^{TB}, I_0^{SB}, γ_t, and γ_s are all determined for different bias regions. The ideality factor n is fixed at 1.5 in this fitting for convenience. This is because nonideal rectification properties are expected in our sample structure. Figure 6 shows the fitting results from direct current *I-V* characteristics for different thickness of MgO in GaAs/MgO/Fe samples at room temperature. In order to extract physically realistic values, the bias-dependent contribution of transport processes, i.e., the different ratio of current-density component of J_{TB} to J_{SB} is obtained first with a different bias region as shown in Fig. 6(a). The data points are the representative estimated values for each local bias region. The ratio tells us which transport process dominates in the bias region. From the fitting, the highest ratio of J_{SB}/J_{TB} is obtained in the high forward bias (above 0.4–0.5 V) region for each sample. In the case of high ratio (>1) of J_{SB}/J_{TB}, transport path of (2) may contribute to J_{SB} together with path (1) due to the increased transparency of tunnel barrier. Particularly, the expression of electron current of the path (2) can be described by Ref. 16 as

$$J = A^{**}T^2 e^{-q\phi_{SB}/kT} e^{-\sqrt{\chi}d}(e^{qV/nkT} - 1), \tag{7}$$

where $\sqrt{\chi}$ and d are the effective evanescent wave number and the barrier thickness, respectively. The other parameters

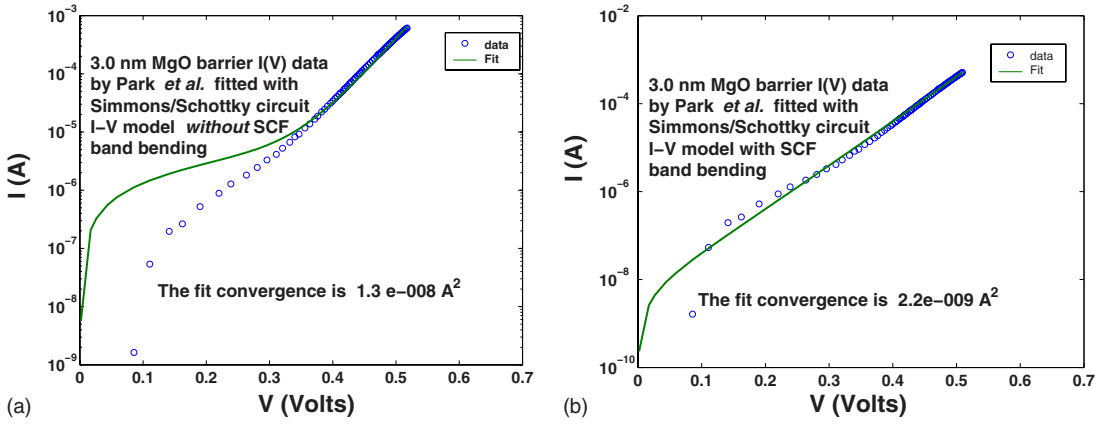

FIG. 4. (Color online) (a) The Simmons/Schottky circuit model fit to the 3.0 nm data without the SCF band bending while using the rigid band diagram at zero bias [Fig. 2(b)]. (b) The Simmons/Schottky circuit model fit to the 3.0 nm data *including* the SCF band bending [see Fig. 2(a)]. The fit convergence is improved by 1 order of magnitude as a result of the inclusion of the SCF band bending to the Simmons/Schottky $I(V)$ fitting model.

are the same as described earlier in Eqs. (2) and (3). As for the 2.75-nm-thick MgO sample, the high (>1) J_{SB}/J_{TB} ratios remain for the entire forward bias region including moderate negative bias. This is mainly due to the larger component of J_{SB} with a relatively small contribution in path (2) compared with J_{TB}. The thin TB sample contains more pinholes in the barrier than in the thicker TB sample. This condition reduces the effective thickness and provides enhanced thermionic emission current component via pinholes.

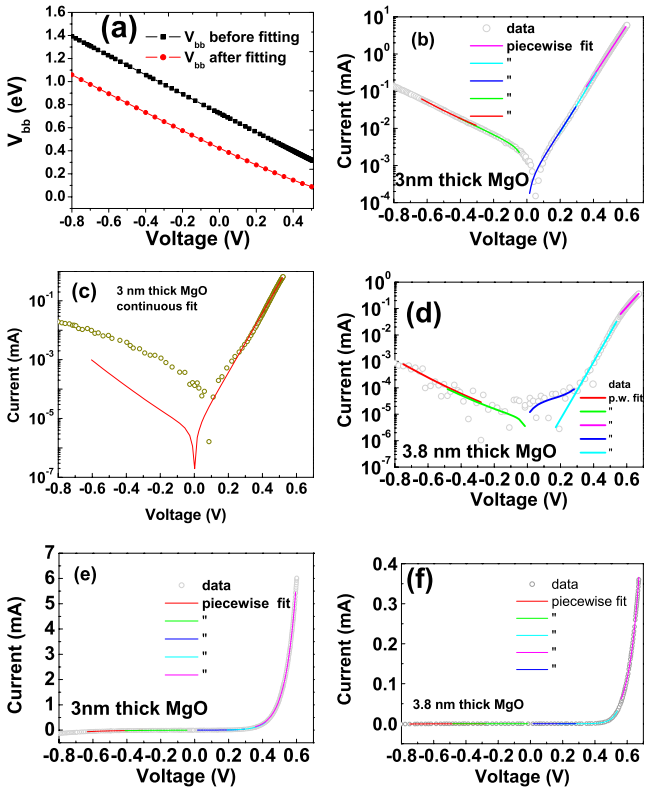

FIG. 5. (Color online) (a) Plot of the effective band bending (V_{bb}) before and after the SCF curve fitting. (b) I-V curve obtained from GaAs/MgO/Fe structure for a MgO thickness of 3 nm wherein the current axis is plotted on a log scale. Sections of the curve are taken out for piecewise fitting and are plotted with the data. (c) The plot of the I-V data with an SCF fit over the entire bias region which indicates a divergence from the model toward around the zero and negative bias region. (d) I-V curve obtained from GaAs/MgO/Fe structure for a MgO thickness of 3.8 nm. Plots (e) and (f) show the data with the current axis on a linear scale.

In the case of 3.8-nm-thick TB sample, the relative contribution of transport path (2) and (3) becomes more significant than for the thinner MgO sample due to the lower probability of the existence of pinholes in general. As decreasing the forward bias (about 0.15 V), the ratios of J_{SB}/J_{TB} abruptly decreases down to about 10^{-4}, indicating greater contribution of J_{TB} [i.e., mostly path (3) plays a role]. If path (2) becomes significant, the ratio of J_{SB}/J_{TB} does not change much, i.e., there exists a balance between J_{SB} and J_{TB} on the basis of the modeling scheme. In physical terms, the interface state tunneling path (3) comprises the tunneling current via the filled interface states and recombination current via the surface holes at the forward bias region. Thus, a significant lowering in the ratio of J_{SB}/J_{TB} at 0.15 V is mainly caused by the current flowing in path (3) in the 3.8-nm-thick TB sample, whereas, in the 3 nm sample, this lowering is less abrupt due to current flow in path (3) and (1). On the other hand, in the negative bias region, the ratio J_{SB}/J_{TB} tends to be lower than 1 in general. The electron transport through the TB into the empty interface states in the GaAs energy band gap contributes to the dominant current component in the path (3) at reverse bias. The interface state tunneling current is proportional to the density of states, D_{it} and is larger than the saturation current in thermionic emission mode, which is independent of negative bias. If D_{it} is constant with energy, the ratio of J_{SB}/J_{TB} is expected to be nearly constant as a function of negative bias and this inference agrees with the fitting results for the 3- and 3.8-nm-thick TB samples as shown in Fig. 6(a). As for the thicker TB case, the tunneling current is attenuated with TB thickness, resulting in reduced J_{TB} [path (3)] compared with the thin TB sample. An abrupt drop of the ratio for 2.75 nm TB sample at −0.54 V is due to the leakage current through the interface states. Thus the interface state tunneling current of

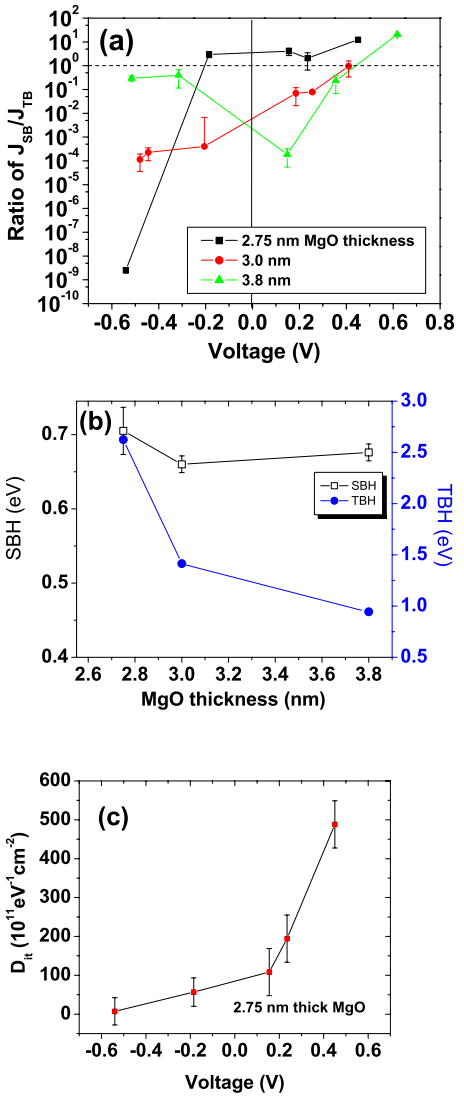

FIG. 6. (Color online) (a) The ratio of thermionic emission current and tunneling current as calculated from the self-consistent *I-V* curve fitting model. (b) TBH and SBH are extracted from the *I-V* fits. (c) The Schottky thermionic model gives a measure of the interface density of states, which are also plotted here as a function of applied bias.

path (3) can enormously contribute to the total current in the reverse bias region.

In Fig. 6(b), the bias-dependent TBH ϕ_{TB}^0 and SBH ϕ_{SB}^0 are plotted. Typical values for ϕ_{SB}^0 are in the range of 0.66–0.7 eV and are nearly independent on TB thickness. Regarding the bias-dependent SBH, ϕ_{SB} shows a decreasing trend at high forward bias (not shown here), contributing to the enhanced J_{SB}/J_{TB} ratio. On the other hand, the TBH, which is reasonably estimated in the negative bias region, tends to decrease from 2.6 to 0.95 eV as the TB thickness increases from 2.75 to 3.8 nm. The values of ϕ_{TB} estimated from the curve fits are dependent upon the bias region which is sampled and this is due to the distortion of the tunnel barrier profile as a function of bias. In the case of the 2.75-nm-thick MgO samples, the estimated TBH of 2.6 eV may result from factors related to the relatively large contribution of interface state leakage current component [see the extremely low bias region of the J_{SB}/J_{TB} ratio plotted in Fig. 6(a)]. Thus, from the fitting, the respective TBHs of 1.4 and 0.95 eV for 3- and 3.8-nm-thick TB samples are reasonable.

Through the analysis of fitting parameters, the density of interface states is also estimated to be about 10^{12}–10^{13} eV^{-1} cm^{-2} at nearly zero bias for all prepared samples, as shown in Fig. 6(c). The higher density of interface states is primarily obtained at high forward bias, whereby the states rise to the energy-band edge in the semiconductor. It induces the increase in D_{it} toward the energy-band edge. The thinner tunnel barrier sample shows higher D_{it} in the negative bias region which can contribute to the interface state tunneling current. In terms of the spin-filtering effects, the density of interface states degrades the efficiency.[25] A lower contribution of interface state tunneling is necessary for efficient spin transport. That is to say, for an effective spin-filtering effect, transport path (2) must dominate by minimizing the interface states tunneling expressed by the path (3).

It is found from the $J(V)$ model analysis that the estimated physical parameters given with respect to the fitted bias region, plausible parameter information can be obtained through the analysis of the dominant transport process for the specific bias region. Our self-consistent fitting model can be used to analyze a wide variety of realistic MIS structures.

IV. CONCLUSIONS

Using a self-consistent fitting model, we have shown that the measured *I-V* characteristics of the GaAs/MgO/Fe structures can be accurately modeled. In order to extract physically realistic parameters, a sectioning technique of the bias region was employed. It was found that the thermionic emission transport prevails over the tunneling in the high forward bias region for the thin MgO tunnel barrier samples. Our results show that the analysis of *I-V* data can be applied generally to MIS structure having thin tunnel barriers. The fittings are largely influenced by the quality of the MgO tunnel barriers. Through the analysis of the primary transport process in a certain bias regions, the characteristic $I(V)$ can be computed exactly, giving information about the surface density of states, relative barrier capacitances, barrier heights, and the ratio of tunneling current to thermionic Schottky emission. These two competing transport mechanisms need to be quantitatively accounted for in order to identify favorable transport regimes for spin filtering and spin injection through insulating barriers.

ACKNOWLEDGMENTS

This work is supported by the KIST-MIT program. M. C. Hickey would like to thank the U.S.-UK Fulbright commission for funding.

*Present address: Department of Material Science and Engineering, University of California at Los Angeles, Los Angeles, California 90095, USA.
†hickey@mit.edu

[1] S. Yuasa and D. D. Djayaprawira, J. Phys. D **40**, R337 (2007).
[2] Z. Diao, D. Apalkov, M. Pakala, Y. Ding, A. Panchula, and Y. Huai, Appl. Phys. Lett. **87**, 232502 (2005).
[3] R. Dave, G. Steiner, J. Slaughter, J. Sun, B. Craigo, S. Pietambaram, K. Smith, G. Grynkewich, M. DeHerrera, J. Åkerman, and S. Tehrani, IEEE Trans. Magn. **42**, 1935 (2006).
[4] E. I. Rashba, Phys. Rev. B **62**, R16267 (2000).
[5] G. Schmidt, D. Ferrand, L. W. Molenkamp, A. T. Filip, and B. J. van Wees, Phys. Rev. B **62**, R4790 (2000).
[6] G. Salis, R. Wang, X. Jiang, R. M. Shelby, S. S. P. Parkin, S. R. Bank, and J. S. Harris, Appl. Phys. Lett. **87**, 262503 (2005).
[7] S. Yuasa, T. Nagahama, A. Fukushima, Y. Suzuki, and K. Ando, Nature Mater. **3**, 868 (2004).
[8] S. S. P. Parkin, C. Kaiser, A. Pachula, P. M. Rice, B. Hughes, M. Samant, and S.-H. Yang, Nature Mater. **3**, 862 (2004).
[9] J. Mathon and A. Umerski, Phys. Rev. B **63**, 220403(R) (2001).
[10] W. H. Butler, X.-G. Zhang, T. C. Schulthess, and J. M. MacLaren, Phys. Rev. B **63**, 054416 (2001).
[11] A. N. Chantis, K. D. Belashchenko, D. L. Smith, E. Y. Tsymbal, M. van Schilfgaarde, and R. C. Albers, Phys. Rev. Lett. **99**, 196603 (2007).
[12] S. Honda, H. Itoh, J. Inoue, H. Kurebayashi, T. Trypiniotis, C. H. W. Barnes, A. Hirohata, and J. A. C. Bland, Phys. Rev. B **78**, 245316 (2008).
[13] H. Dery and L. J. Sham, Phys. Rev. Lett. **98**, 046602 (2007).
[14] Y. J. Park, M. J. van Veenhuizen, J. S. Moodera, C. H. Perry, and D. Heiman, APS March Meeting, BAPS.2007.MAR.B12.00004 (2007).
[15] X. Jiang, R. Wang, R. M. Shelby, R. M. Macfarlane, S. R. Bank, J. S. Harris, and S. S. P. Parkin, Phys. Rev. Lett. **94**, 056601 (2005).
[16] H. C. Card and E. H. Rhoderick, J. Phys. D **4**, 1589 (1971).
[17] H. C. Card and E. H. Rhoderick, J. Phys. D **4**, 1602 (1971).
[18] L. B. Freeman and W. E. Dahlke, Solid-State Electron. **13**, 1483 (1970).
[19] F. Xu, H. Pan, W. Zhang, G. Wang, Z. Li, and P. Xu, J. Electron Spectrosc. Relat. Phenom. **144-147**, 385 (2005).
[20] J. G. Simmons, J. Appl. Phys. **34**, 1793 (1963).
[21] W. F. Brinkman, R. C. Dynes, and J. M. Rowell, J. Appl. Phys. **41**, 1915 (1970).
[22] C. Nam, B. G. Ng, F. J. Castaño, M. D. Mascaro, and C. A. Ross, Appl. Phys. Lett. **94**, 082501 (2009).
[23] Y.-N. Xu and W. Y. Ching, Phys. Rev. B **43**, 4461 (1991).
[24] M. S. Sze, *The Physics of Semiconductor Devices* (Wiley, New York, 1981).
[25] R. Jansen, M. W. J. Prins, and H. van Kempen, Phys. Rev. B **57**, 4033 (1998).
[26] I.-H. Tan, G. L. Snider, L. D. Chang, and E. L. Hu, J. Appl. Phys. **68**, 4071 (1990).